Influence of particle size and density, and channel velocity on the deposition patterns around a circular patch of model emergent vegetation

Citation: Shi, Ying, et al. "Influence of Particle Size and Density, and Channel Velocity on the Deposition Patterns Around a Circular Patch of Model Emergent Vegetation." Water Resources Research 52, 2 (February 2016): 1044–1055 © 2016 American Geophysical Union

As Published: http://dx.doi.org/10.1002/2015WR018278

Publisher: American Geophysical Union

Persistent URL: http://hdl.handle.net/1721.1/111615

Version: Final published version: final published article, as it appeared in a journal, conference proceedings, or other formally published context

AGU PUBLICATIONS

Water Resources Research

RESEARCH ARTICLE
10.1002/2015WR018278

Key Points:
- Resuspension drives the spatial deposition pattern near finite patches of vegetation
- Spatial patterns in net deposition are categorized by the ratio of channel shear velocity to critical shear velocity (u_*/u_{*c})
- Preferential accumulation of fine particles in the wake behind a finite patch of vegetation occurs when $u_*/u_{*c} = 0.7$–3

Correspondence to:
H. M. Nepf,
hmnepf@mit.edu

Citation:
Shi, Y., B. Jiang, and H. M. Nepf (2016), Influence of particle size and density, and channel velocity on the deposition patterns around a circular patch of model emergent vegetation, *Water Resour. Res.*, *52*, 1044–1055, doi:10.1002/2015WR018278.

Received 23 OCT 2015
Accepted 18 JAN 2016
Accepted article online 23 JAN 2016
Published online 14 FEB 2016

Influence of particle size and density, and channel velocity on the deposition patterns around a circular patch of model emergent vegetation

Ying Shi[1,2], Beihan Jiang[2], and Heidi M. Nepf[2]

[1]Department of Hydraulic Engineering, Tsinghua University, Beijing, China, [2]Department of Civil and Environmental Engineering, Massachusetts Institute of Technology, Cambridge, Massachusetts, USA

Abstract This laboratory study examined the influence of particle size and density, and channel velocity on the spatial deposition pattern around an emergent (extending through the entire water depth), circular patch of model vegetation located at the center of a channel. Three flow conditions and three particles of different size and density were considered. Across all particle and velocity conditions, three basic deposition patterns were observed: (1) high deposition in the patch wake and low deposition in the zones adjacent to the patch; (2) high deposition in both the wake and adjacent zones; and (3) low deposition in both the wake and adjacent zones. The observed deposition pattern correlated with the ratio of channel shear velocity (u_*) to critical shear velocity (u_{*c}). Specifically, for $u_*/u_{*c} < 0.7$ or $u_*/u_{*c} > 3$, the deposition was high (or low, respectively) over the entire channel with little difference between the wake and adjacent regions. In contrast, for $0.7 < u_*/u_{*c} < 3$ divergence in net deposition between the wake and the adjacent zones occurred, with higher net deposition in the wake and lower net deposition in the adjacent zones. The peak divergence was observed at $u_*/u_{*c}=1.6$. The deposition patterns were more closely correlated with the ratio u_*/u_{*c} than with w_s/u_* (with w_s the particle settling velocity), suggesting that the spatial variation in net deposition was driven by resuspension (associated with u_{*c}) and not settling (associated with w_s).

1. Introduction

Vegetation is a common feature in shallow aquatic systems and provides several ecosystem functions, such as improving water quality [*Schulz et al*., 2003; *Cotton et al*., 2006], stabilizing the bed [*Bouma et al*., 2007; *Rominger et al*., 2010], and promoting habitat diversity [*Crowder and Diplas*, 2000; *Hafs et al*., 2014]. Generally, vegetation is understood to reduce flow and enhance deposition [*Kouwen and Unny*, 1975; *Stephan and Gutknecht*, 2002], and it has been shown to control the transport of particles through a channel [*Jones et al*., 2012]. Finite patches of vegetation have been studied to understand the biogeomorphic feedbacks between vegetation, flow, deposition, and further growth [*Nepf*, 2012; *Gurnell et al*., 2012; *Gurnell* 2014; *Marion et al*., 2014]. In particular, the deposition of fine material, rich in nutrients and organic matter, is considered a precursor to growth [*Cotton et al*., 2006; *Gurnell et al*., 2012; *Jones et al*., 2012]. Both positive and negative feedbacks between vegetation, flow, and deposition have been observed, i.e., some regions near existing vegetation experience net deposition that would promote growth, while other regions near existing vegetation experience net erosion, which would tend to inhibit growth. For example, enhanced net deposition has been observed in the wake downstream of a vegetation patch, while enhanced net erosion has been observed at the lateral edge of a patch, and within the patch, both net deposition and net erosion have been observed [*Cotton et al*., 2006; *Bouma et al*., 2007; *Follett and Nepf*, 2012; *Tanaka and Yagisawa*, 2010; *Chen et al*., 2012; *Ortiz et al*., 2013]. Thus, the presence of a finite patch of vegetation creates spatial heterogeneity in the net deposition that may drive the pattern of future vegetation growth [*Kondziolka and Nepf*, 2014; *Meire et al*., 2014].

Whether net deposition or net erosion occurs depends on the relative contributions of the individual processes of resuspension and sedimentation (deposition). The resuspension of particles depends on the bed shear stress, τ_0.

$$\tau_0 = \rho u_*^2 \quad (1)$$

where ρ is the fluid density and u_* is the shear velocity. Resuspension occurs when the bed shear stress exceeds a critical stress for incipient motion (τ_c), which defines a critical shear velocity,

$$u_{*c} = (\tau_c/\rho)^{1/2} \quad (2)$$

The shear velocity (u_*) also characterizes the strength of turbulent eddies that act to keep particles in suspension, which can influence deposition. The deposition of particles also depends on the particle settling velocity, w_s. In the present study, we consider how these three velocity scales, u_*, u_{*c}, and w_s, influence the pattern of net deposition of suspended material, and in particular the degree of spatial heterogeneity in net deposition observed near finite patches of vegetation. Although we recognize that bed load transport also provides important feedbacks to patch structure [e.g., *Bouma et al*., 2007], in this study, we focus on material carried as suspended load (fine material rich in nutrients and organic matter), and we look for the conditions for which the suspended load preferentially deposits near the vegetation, providing a positive feedback to continued growth.

Recently, *Ortiz et al*. [2013] observed that the spatial heterogeneity in net deposition generated by a finite patch of model vegetation increased with increasing channel velocity. Specifically, as the channel velocity increased less material was deposited in the open channel, making more material available to deposit in the wake downstream of the patch, such that net deposition increased in the wake. Thus, as the channel velocity increased, the net deposition in the open channel and the wake diverged, leading to higher spatial heterogeneity in the net deposition pattern. *Ortiz et al*. [2013] connected this result to the ratio of settling velocity (w_s) to channel shear velocity (u_*), noting that as w_s/u_* decreased, the spatial standard deviation in net deposition increased. This ratio represents the competing influence of settling and turbulent diffusion on the distribution of particles in the water column. It is related to the Rouse number ($R_o = w_s/\beta_s \kappa u_*$), in which κ $(=0.4)$ is the von Karman constant and β_s is a constant of approximately 1 [*Julien*, 1995, chap. 10.4]. Smaller values of R_o are associated with more uniform vertical profiles of sediment concentration, as turbulence mixes the particles upward away from the bed, making the particles less available for deposition [*Julien*, 1995]. So, it is reasonable to expect a decrease in net deposition in the channel as w_s/u_* and R_o decrease, which would occur as channel velocity increases, as observed by *Ortiz et al*. [2013, Figure 13a]. However, *Ortiz et al*. [2013] only considered a single particle size and density, so that the change in w_s/u_* only reflected changes in channel velocity. Hence, their result cannot be confidently extrapolated to other sediment sizes or densities (i.e., other values of w_s). In this study, we vary particle size and density, as well as the channel velocity, to examine whether w_s/u_* works as a universal predictor of deposition pattern. Further, the critical shear velocity, u_{*c}, also influences net deposition. Specifically, if the channel shear velocity (u_*) exceeds the critical shear velocity (u_{*c}), then deposition will be inhibited, because particles touching down at the bed can be immediately resuspended. Since the critical shear velocity (u_{*c}) is a function of particle size (d_p) and density (ρ_p), our consideration of different particle size and density and different channel velocity will produce a range of u_*/u_{*c} values. We can then examine whether w_s/u_* or u_*/u_{*c} is the better predictor of spatial heterogeneity in net deposition measured near a patch of model vegetation.

2. Methods

2.1. Experimental Setup

Experiments were conducted in a 16 m long, 1.2 m wide flume in which both the water and sediment were recirculated (Figure 1). The bed of the flume was horizontal. A weir at the downstream end of the flume controlled the water depth. PVC baseboards, perforated with a staggered arrangement of holes, covered the bed of the test section. A circular patch of model vegetation was constructed in the center of the flume using rigid wooden circular cylinders. The patch diameter (D) was 20 cm, which was much smaller than the flume width (120 cm), so that the walls had little impact on the flow adjacent to the patch [e.g., *Follett and Nepf*, 2012]. The cylinder diameter (d) was 6.4 mm, which falls in the range of real emergent vegetation stems, $d=0.1$–1 cm [*Valiela et al*., 1978; *Leonard and Luther*, 1995; *Lightbody and Nepf*, 2006]. Given that we focused on emergent vegetation, the flow field was approximately two-dimensional, with the flow diversion and dominant shear layers occurring in the horizontal plane [*Chen et al*., 2012; *Follett and Nepf*, 2012]. The stem density within the patch, described by the frontal area per volume, $a=nd$, was 25 m^{-1}, with n the

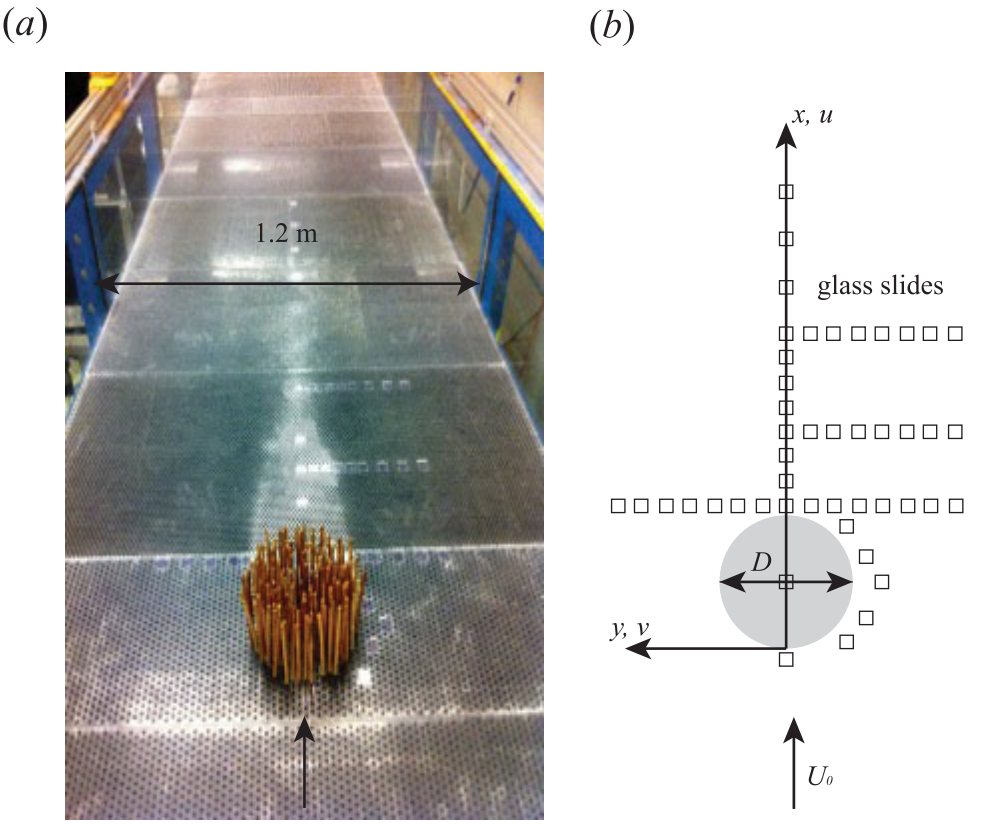

Figure 1. Top view of experimental set up. Flow is from bottom to top, as indicated by black arrow. (a) Circular patch of model vegetation located at mid channel. Patch diameter (D) was 0.2 m and flume width was 1.2 m. Image taken following a deposition experiment. Elevated deposition, evident by the white color, occurred in a triangular region that corresponded to the wake downstream of the patch. A similar pattern of deposition has been observed in the field (Photos 1 and 3 in *Tsujimoto* [1999]). (b) Gray circle represents the model vegetation patch. 2.5 cm × 2.5 cm glass slides were placed in the adjacent zone and wake zone. $x=0$ was at the upstream edge of the patch and $y=0$ was at the centerline of the patch and the flume. Figure not to scale.

number of stems per bed area within the patch. For an emergent patch, the magnitude of flow diversion and the strength of the lateral shear layers are set by the nondimensional flow blockage (aD). In this case, $aD=5.1$, corresponding to high flow blockage [*Rominger and Nepf*, 2011; *Chen et al.*, 2012]. The solid volume fraction within the patch was $\phi=\pi ad/4=0.13$, which was representative of densities found in real aquatic vegetation [*Nepf*, 2012].

2.2. Velocity Measurements

The coordinate system was defined as x in the streamwise direction, with $x=0$ at the leading edge of the patch, y in the lateral direction, with $y=0$ at the center of the patch and flume, and z in the vertical direction with $z=0$ at the bed. Velocity measurements were taken from $5D$ upstream of the patch to $30D$ downstream of the patch using a Nortek Vectrino (acoustic Doppler velocimeter, ADV). At each position, the velocity was measured at mid depth for 240 s with a sampling rate of 25 Hz. In previous studies in the same flume, measurements at mid depth were shown to be within 5% of the depth-averaged velocity [*White and Nepf*, 2007; *Chen et al.*, 2012; *Ortiz et al.*, 2013]. Three components of instantaneous velocity (u, v, w) were collected at each point, with u the velocity in the streamwise direction, v the lateral velocity, and w the vertical velocity. Each velocity record was decomposed into time-averaged components $(\bar{u},\bar{v},\bar{w})$ and fluctuating components (u',v',w'). The average velocity upstream of the patch was defined as the reference velocity, U_0. Three flow conditions were considered ($U_{01}=4.9\pm0.3$ cm/s, $U_{02}=9.6\pm0.3$ cm/s, $U_{03}=19.0\pm0.3$ cm/s). The water depth measured at the upstream end for these three cases was 13.4 ± 0.2, 14.0 ± 0.2, and 11.2 ± 0.2 cm, respectively. The bed friction coefficient ($C_f=(u_*/U_0)^{1/2}=0.006$) was estimated previously for the same baseboards, with u_* determined by fitting vertical profiles of velocity to a log profile [*Zong and Nepf*, 2010]. The same coefficient was used in this study to estimate the channel shear velocity as

Table 1. Summary of Flow Parameters[a]

Case	D (cm)	a (m^{-1})	aD	ϕ (%)	U_0 (cm/s)	u_* (cm/s)	U_1/U_0	U_2/U_0	U_{adj}/U_0	U_{wake}/U_0	L_1 (cm)
This study	20	25	5.1	13	4.9 ± 0.3	0.38	0.03 ± 0.01	1.23 ± 0.04	1.1 ± 0.2	0.12 ± 0.1	60
					9.6 ± 0.3	0.74	0.05 ± 0.02	1.23 ± 0.02	1.0 ± 0.3	0.26 ± 0.2	60
					19.0 ± 0.3	1.47	0.04 ± 0.02	1.23 ± 0.03	1.0 ± 0.2	0.19 ± 0.1	60
Chen	20	23	4.6	12	9.8		0.06	Not given			60
Zong	22	29	6.3	14	9.7		0.03 ± 0.01	1.3 ± 0.03			70

[a]Uncertainty in U_1/U_0 and U_2/U_0 reflects instrument error. Uncertainty in U_{adj}/U_0 and U_{wake}/U_0 is standard deviation among the measuring points in the defined area.

$u_* = \sqrt{C_f}U_0$ (see Table 1). However, we note that as the flow adjusts around the patch the local velocity profiles will not be logarithmic, so that this estimator is only approximate.

2.3. Deposition Experiment

Three different particles, with different diameter (d_{50}) and density (ρ_p) were used in the experiments (Table 2). The particles were spherical glass beads. The E5000 and E4000 particles were solid, and the V2162 particles were hollow. Because of their spherical shape, the settling velocity can be predicted by Stokes' law [*Lamb*, 1993]:

$$w_s = (\rho_p - \rho) g d_{50}^2 / 18\mu \tag{3}$$

where μ is the dynamic viscosity of the fluid and g is gravitational acceleration. The critical shear velocity (u_{*c}) for each particle was estimated from the critical Shields parameter, τ_{*c} [e.g., *Julien*, 1995]:

$$\tau_{*c} = \frac{\tau_c}{(\rho_p - \rho) g d_p} \tag{4}$$

where d_p is the size of the spherical particle, which is usually taken as the median diameter (d_{50}). The value of the critical Shields parameter, τ_{*c}, was estimated from the non-dimensional particle number, $d_* = \left[\frac{(\rho_p - \rho)g}{\rho \nu^2}\right]^{1/3} d_p$, with "$\nu$" the kinematic viscosity, using equation (7.4) in *Julien* [1995]. The critical shear velocity, u_{*c}, was then calculated from equations (2) and (4) (values given in Table 2). Following the discussion given in *Ortiz et al*. [2013], the particles were chosen to mimic the transport of fine organic matter in the field by scaling the ratio of settling velocity to shear velocity. In the field $w_s/u_* = 0.02$–0.3 [*Ortiz et al*. 2013]. In this study, $w_s/u_* = 0.007$–0.28. The particle size was not geometrically scaled.

Net deposition was measured using glass slides (2.5 cm × 2.5 cm) placed on the bed of the flume. The clean and dry slides were weighed before placement. The placement was arranged based on the flow characteristics with one slide ahead of the patch, four adjacent to the patch, three rows of slides behind the patch, and one line along the centerline of the flume and patch (Figure 1). To initiate a deposition experiment, 600 g of particles was first mixed with water in a small container, and the mixture was added to the tail box of the flume. The heavier particles (E5000 and E4000) mixed to a uniform concentration over the flume within 5 min while the lighter particle (V2162) required 40 min, because these particles had a tendency to remain at the surface and thus required additional mixing. Once mixed, the flume was run for 4 h, after which the pump was slowly stopped and the weir was lifted 4 cm off the bed to slowly drain the water from the test section. It took 20 min to stop the pumps and drain the water from the test section. The 4 h duration was selected based on previous similar experiments [*Ortiz et al*. 2013] to be long enough to develop a measurable signal on the slides but short enough to facilitate multiple runs. The slides were left to air dry in the channel for at least 2 days. Afterward, the slides were placed in an oven at 50°C for 4 h to remove the moisture, and then they were reweighed. The net deposition at each position was calculated by the difference in weight before and after the experiment, divided by the area of the glass slide. The measurement

Table 2. Particle Information[a]

Name	d_{50} (μm)	ρ_p/ρ	u_{*c} (mm/s)	w_s (mm/s)
E5000	10	2.5	6.6	0.1
E4000	24	2.5	8.7	0.5
V2162	45	1.02	1.6	0.02

[a]Values of d_{50} and ρ_p/ρ were provided by the company. The E5000, E4000, and V2162 contained the following size ranges: 1–26, 1–89, and 1–106 μm, respectively. E5000 and E4000 were purchased from the Spheriglass product line from Potters Industry (Valley Forge, PA, USA). V2162 was from Evonik industry (Parsippany, NJ, USA). u_{*c} was calculated from equations (2) and (4), using τ_{*c} estimated using equation (7.4) in *Julien* [1995]. w_s was calculated from equation (3).

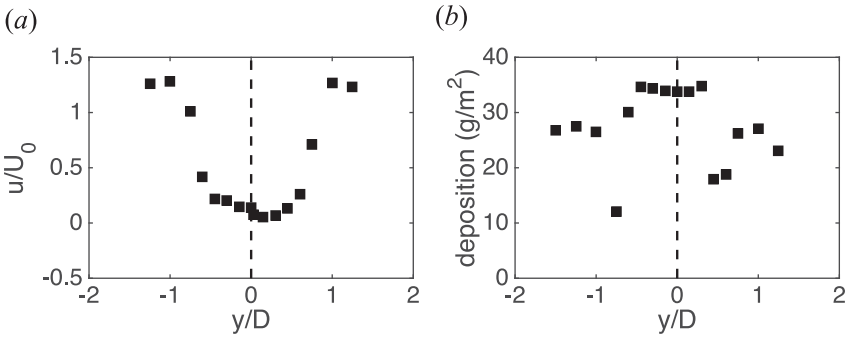

Figure 2. (a) Lateral profile of streamwise velocity measured at $x=2.5D$, $y=-1.3D$ to $1.3D$, $U_0=9.6$ cm/s. The uncertainty in the velocity was 0.1 cm/s; (b) Lateral profile of net deposition measured at $x=1.25D$, $y=-1.5D$ to $1.5D$, $U_0=9.6$ cm/s, E4000. The uncertainty in the deposition measurement was 1.8 g/m^2.

location was defined as the center point of the glass slide. Each deposition experiment was repeated twice and the replicate standard error was used to define the uncertainty at each measurement point. Because of a limited particle supply, the lightest particles (V2162) could not be repeated, and for these cases we estimated uncertainty from the standard error among all points. Control experiments were also conducted with the same particle, channel velocity, and placement of the slides, but with no patch in the flume. Finally, in a preliminary experiment, both the velocity and deposition were measured on a lateral transect that spanned the flume over both sides of the patch. These measurements confirmed that the flow and deposition were symmetric across the centerline of the patch and flume (Figure 2). For subsequent experiments, measurements were just made over half of the flume.

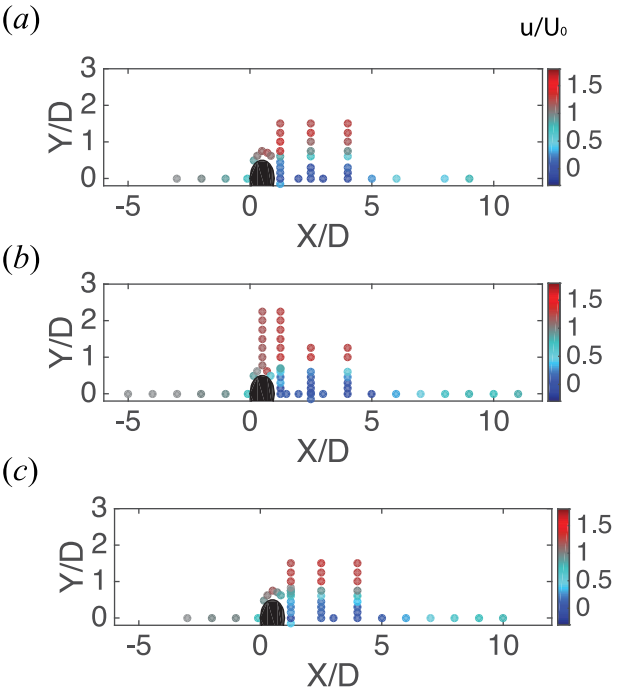

Figure 3. Left-side of channel ($y>0$) showing the distribution of velocity normalized by channel velocity U_0. Flow is left to right, with $x/D=0$ at the leading edge of the patch, which is shown by a black semicircle. (a)–(c) correspond to $U_0=4.9$, 9.6, and 19 cm/s, respectively. The dot locations correspond to measurement locations, and the color of each dot indicates the magnitude of the normalized velocity (u/U_0), as shown in the color bar.

3. Results

3.1. Flow characteristics

The distribution of streamwise velocity (u) is depicted in Figure 3. The individual dots are located at the measurement positions, and the color of the dot indicates the magnitude of the normalized velocity u/U_0, as shown by the color bar. The three rows (Figures 3a–3c) correspond to the three velocity conditions ($U_0=4.9$, 9.6, and 19 cm/s, respectively). The three velocity conditions exhibited similar variation in normalized velocity. Specifically, there was a region of diminished velocity (Figure 3, dark blue dots) directly downstream from the patch and a region of enhanced velocity (Figure 3, red dots) adjacent to the patch. Further, the longitudinal and lateral profiles of the normalized velocity (u/U_0) were essentially identical for the three velocity conditions (Figures 4b and 4c). The distribution of velocity measured in our study was also consistent with the description of flow past porous patches given in previous studies. The main characteristics are summarized in Figure 4a. High flow resistance within the patch causes upstream flow to divert laterally away

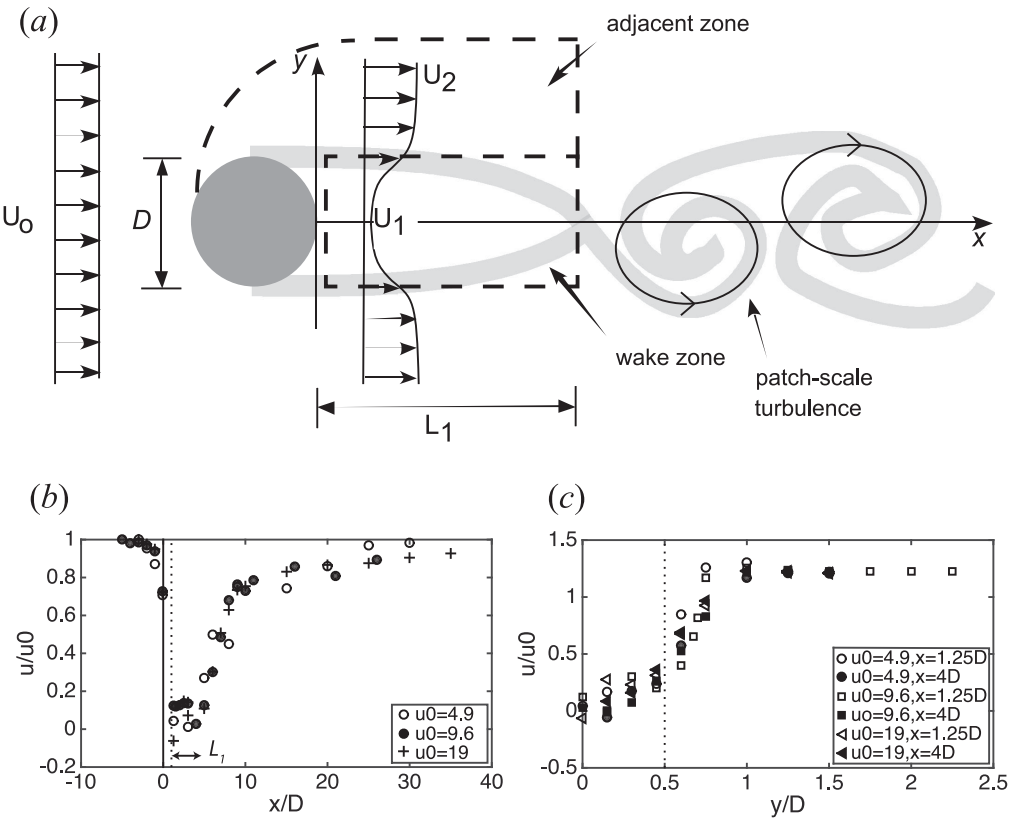

Figure 4. (a) Schematic diagram of flow past circular patch of model vegetation, showing the upstream velocity (U_0), steady wake velocity (U_1), velocity adjacent to wake (U_2), and the length of the steady wake region (L_1). Patch-scale turbulence forms at the end of the steady wake, generating mixing that produces the increasing centerline velocity beyond this point. The labeled regions marked by dashed lines indicate the adjacent and wake zones defined for the deposition experiments. (b) Longitudinal profiles of normalized velocity (u/U_0) along the centerline of the flume and patch (y = 0) for U_0=4.9, 9.6, 19 cm/s. Patch located between the solid vertical line at x=0 and the dashed vertical line at x=D. (c) Lateral profiles of normalized velocity between y=0 and 2.25D, and at two streamwise positions, x=1.25D and x=4D for all three velocity conditions. Vertical dashed line at y/D = 0.5 indicates the lateral edge of patch.

from the patch, resulting in higher velocity ($U_2 > U_0$) in the region adjacent to the patch and lower velocity ($U_1 < U_0$) in the wake directly behind the patch [*Zong and Nepf*, 2011; *Chen et al.*, 2012]. When the shear layers meet, a von Karman vortex street is formed at distance L_1 behind the patch, and this patch-scale turbulence produces the rapid increase in mean velocity beyond this point (Figure 4b). Together, the velocity data shown in Figures 3, 4b, and 4c demonstrate the similarity in the velocity field, when scaled by the upstream velocity U_0.

To make a consistent comparison between the net deposition within the region of diminished velocity in the wake and the region of enhanced velocity adjacent to the patch, we used the measured velocity field to define a wake zone and adjacent zone (labeled in Figure 4a), which were subsequently used across all experimental conditions. The following details were considered in defining these two zones. The streamwise velocity within the wake (U_1) remained constant over length scale L_1. Beyond L_1 patch-scale turbulence (Figure 4a) causes the wake velocity to increase and may inhibit deposition [see *Chen et al.*, 2012, for discussion], so that we chose the length of the wake zone to be L_1. This length scale can be predicted from the growth of a plane shear layer [*Zong and Nepf*, 2011]:

$$L_1 = 2.5D(1+U_1/U_2)/(1-U_1/U_2) \approx 2.5D(1+U_1/U_0)/(1-U_1/U_0) \quad (5)$$

Since U_1/U_0 is only a function of flow blockage (aD) [*Chen et al.*, 2012], all three cases have the same L_1. The measured velocity profiles (Figure 4b) and equation (5) both indicated L_1=3D, and this was used to define the wake zone, i.e., the wake zone extended from x=D to x=4D. The width of the wake zone was defined as the region within which the velocity was laterally uniform at U_1. As shown in the lateral profiles (Figure 4c), the

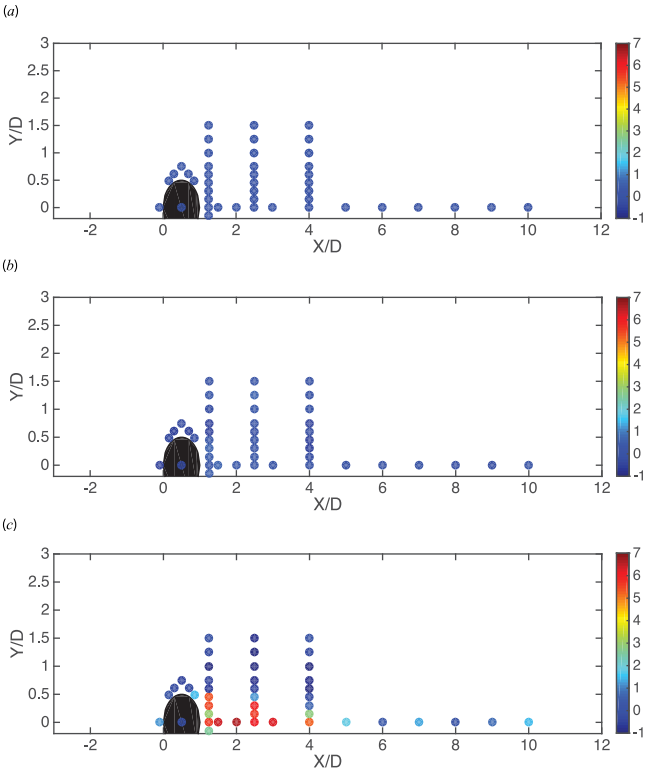

Figure 5. Examples of the three deposition patterns observed with patches. The position of the dot corresponds to the measurement location and the color of the dot corresponds to the magnitude of normalized net deposition, which was calculated as the difference between the measured net deposition with patch and without patch (control) at that location, normalized by the spatial mean deposition in the control. Control experiments were conducted with the same placement of slides. The color bar indicates the value of normalized deposition at each measurement point. (a) Pattern 1 (uniform high deposition) for heaviest particle E4000, w_s = 0.5 mm/s, U_0 = 4.9 cm/s. The control spatial mean deposition was 26.3±1.6 (SD) g/m^2. (b) Pattern 2 (uniform low deposition) for lightest particle V2162, w_s = 0.02 mm/s, U_0 = 9.6 cm/s. The spatial mean deposition was 2.8±1.1(SD) g/m^2. (c) Pattern 3 (high wake deposition) for mid weight particle E5000, w_s = 0.1 mm/s, U_0 = 19 cm/s. The control spatial mean deposition was 3.3±0.9 (SD) g/m^2.

wake velocity (U_1) extended to $y = 0.5D$, corresponding to the edge of the patch, and then increased to a higher velocity (U_2) at $y = D$. Based on this, the width of the wake zone was defined as $y = -0.5D$ to $0.5D$ (labeled in Figure 4a). The adjacent zone was defined as the region of elevated velocity to the side of the patch, which began at the leading edge of the patch and extended to the end of the wake zone, i.e., $x = 0$ to $x = 4D$. To simplify the comparison, we chose the adjacent region to have a width similar to the wake, i.e., width D, extending from $y = 0.5D$ to $y = 1.5D$ (labeled in Figure 4a). This choice was supported by recent numerical simulations, which showed the region of elevated velocity adjacent to an emergent patch extended laterally over a distance comparable to the wake width [*de Lima et al*., 2015, Figure 5].

The average velocity in the wake, U_{wake}, and in the adjacent zone, U_{adj}, was found by averaging all measurements of velocity in the wake zone and adjacent zone, respectively, as defined above (Table 1). Note that because of the averaging area chosen for U_{wake} and U_{adj}, these values differ from U_1 and U_2 defined in *Zong and Nepf* [2011] and *Chen et al*. [2012] (see Table 1). The shear velocity in the wake and adjacent zone was estimated from the bed friction coefficient, $U_{*wake} = \sqrt{C_f} U_{wake}$ and $U_{*adj} = \sqrt{C_f} U_{adj}$, respectively.

3.2. Deposition Patterns

Across all particle and velocity conditions, we observed three basic deposition patterns: uniform high net deposition, uniform low net deposition, and spatially heterogeneous net deposition, with higher deposition in the wake. These patterns are shown in Figures 5a–5c, respectively. The figures show the normalized net deposition, which is calculated as the difference between the measured net deposition with the patch and without the patch (control) at particular slide position, normalized by the spatial mean deposition in the control. For example, Pattern 1 (uniform high net deposition, Figure 5a) occurred for the heaviest particle (E4000, w_s = 0.5 mm/s) at the lowest velocity (U_0 = 4.9 cm/s), for which the spatial average net deposition was $Dep_{flume} = 26.3\ \mathrm{gm}^{-2}$ and the spatial standard deviation was $SD = 2.1\ \mathrm{gm}^{-2}$, i.e., spatial variation was less than 8% of the mean. The high level of net deposition suggested that resuspension was minimal. The control for this case exhibited a similar magnitude of spatial mean and spatial deviation in net deposition ($Dep_{flume\ control} = 26.3\ \mathrm{gm}^{-2}$, $SD = 1.6\ \mathrm{gm}^{-2}$), indicating that the patch had little influence on the pattern of deposition. Pattern 2 (Figure 5b) occurred for the lightest particle (V2162, w_s = 0.02 mm/s) at the middle velocity (U_0 = 9.6 cm/s), for which the net deposition was significantly smaller in magnitude compared to Pattern 1 ($Dep_{flume} = 2.8\ \mathrm{gm}^{-2}$, $SD = 1.1\ \mathrm{gm}^{-2}$), suggesting resuspension was present. A key point to note in both Pattern 1 and Pattern 2 was that the deposition within the wake zone and within the adjacent zone were similar in magnitude (Figures 5a and 5b). In contrast, in Pattern 3 the net deposition was spatially heterogeneous. For

Table 3. Summary of Deposition Parameters[a]

					Dep_{flume} (g/m^2)		Dep_{wake}	Dep_{adj}
Particle Name	U_0 (cm/s)	u_* (mm/s)	u_*/u_{*c}	w_s/u_*	Avg ± SE	SD	Avg ± SE	Avg ± SE
E5000	4.9	3.8	0.58	0.026	16.0 ± 0.5	3.8	15.8 ± 0.6	15.6 ± 0.9
	4.9				11.0 ± 0.5	3.9	10.9 ± 0.9	10.5 ± 0.9
	9.6	7.4	1.12	0.014	16.0 ± 0.8	5.5	16.9 ± 1.2	11.6 ± 0.8
	9.6				13.8 ± 0.8	5.5	14.5 ± 1.1	8.9 ± 0.7
	19	14.7	2.23	0.007	9.0 ± 1.2	8.8	19.0 ± 2.0	2.6 ± 0.4
	19				8.3 ± 1.3	9.0	18.0 ± 2.0	2.0 ± 0.3
E4000	4.9	3.8	0.44	0.13	25.8 ± 0.3	2.1	25.8 ± 0.5	26.5 ± 0.2
	4.9				26.7 ± 0.3	2.2	26.5 ± 0.5	27.7 ± 0.2
	9.6	7.4	0.85	0.07	24.1 ± 1.1	8.1	30.7 ± 1.1	18.6 ± 1.5
	9.6				28.0 ± 0.8	6.0	32.6 ± 0.9	24.4 ± 1.1
	19	14.7	1.69	0.03	8.2 ± 1.7	12.1	21.1 ± 2.9	0.9 ± 0.2
	19				8.9 ± 1.9	13.5	22.7 ± 3.5	1.0 ± 0.3
V2162	9.6	7.4	4.63	0.003	2.8 ± 0.1	1.1	3.2 ± 0.2	2.7 ± 0.2
	19	14.7	9.19	0.001	7.2 ± 1.1	8.1	7.0 ± 0.3	7.9 ± 0.3

[a] U_0 is the channel-average velocity; $u_* = \sqrt{C_f}U_o$ is the channel shear velocity; u_{*c} is the critical shear velocity; w_s is the particle settling velocity (equation (3)); Dep_{flume} and SD are the spatial average and spatial standard deviation in net deposition including all measurements in the channel; Dep_{wake} is the average deposition in the wake zone; Dep_{adj} is the average deposition in the adjacent zone. Uncertainty in net deposition is standard error (SE).

example, Figure 5c shows the mid weight particle E5000 (w_s = 0.1 mm/s) with U_0 = 19.6 cm/s. In this case, the net deposition in the adjacent zone (2.3 gm^{-2}, average of replicates in Table 3) was significantly lower than that in the wake zone (18.5 gm^{-2}, average of replicates in Table 3), creating a spatial heterogeneity (SD) of comparable magnitude to the mean (8.7 ± 8.9(SD) gm^{-2}). The same particle and flow condition with no patch exhibited less spatial heterogeneity, with a spatial mean and spatial deviation of 3.3 ± 0.9(SD) gm^{-2}. The difference between these deposition values demonstrated that for this particle and flow condition the presence of the patch generated significant changes in the spatial pattern of net deposition (Pattern 3).

The three patterns of deposition can be explained by comparing the critical shear velocity associated with the individual particles, u_{*c}, to the shear velocity in the wake (U_{*wake}) and in the adjacent zone (U_{*adj}). In Figure 6, the critical shear velocity for each particle type (calculated from equations (2) and (4)) is plotted as a colored horizontal line (values given in Table 2). The colored markers represent U_{*adj} (square) and U_{*wake} (triangle) for the specific experimental runs depicted in Figure 5, as labeled in Figure 6. Note that U_{*adj} is similar to u_*, because the adjacent zone defined in Figure 4 includes a range of velocity, from values less than to greater than U_0 with a mean close to U_0. First, for Pattern 1 (uniform high net deposition for the heaviest particle E4000 at 4.9 cm/s), the associated shear velocities (u_{*c}, U_{*wake}, U_{*adj}) are shown in red in Figure 6. For this case, both U_{*wake} (red triangle) and U_{*adj} (red square) were below u_{*c} for E4000 (red horizontal line), suggesting that resuspension would be negligible everywhere in the channel. In the absence of resuspension, net deposition should be uniform in the channel, with no difference between the wake and adjacent zones, which was consistent with the observed net deposition pattern (Figure 5a). Second, for Pattern 2 (uniform low net deposition for the lightest particle V2162 at 9.6 cm/s), the associated shear velocities are shown in green in Figure 6. For this case, both U_{*wake} (green triangle) and U_{*adj} (green square) were above the u_{*c} value for V2162 (green horizontal line),

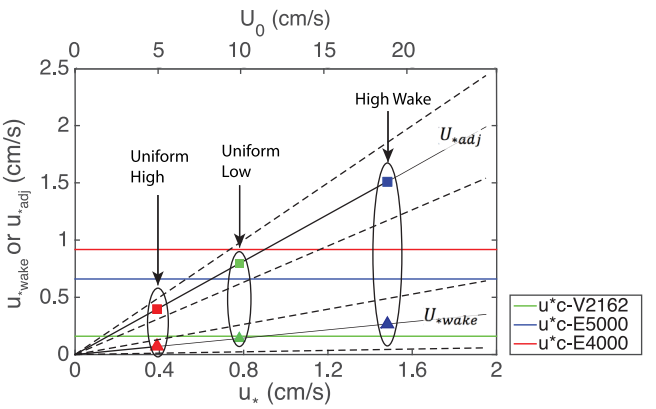

Figure 6. Wake shear velocity ($U_{*wake} = \sqrt{C_f}U_{wake}$) shown with triangles and adjacent shear velocity ($U_{*adj} = \sqrt{C_f}U_{wake}$) shown with squares, as a function of channel shear velocity ($u_* = \sqrt{C_f}U_0$, bottom axis) and as a function of channel velocity, U_0 (upper axis). The solid black line is the best fit through the wake and adjacent shear velocity points, and the dashed lines capture the variability within each zone (see Table 1). The critical shear velocity (u_{*c}) associated with each particle is shown with a colored horizontal line defined in the legend. The values of U_{*wake} (triangles) and U_{*adj} (squares) are plotted in the same color as the associated particle critical shear velocity and labeled with the corresponding deposition pattern from Figure 5: "Uniform High," "Uniform Low," and "High Wake."

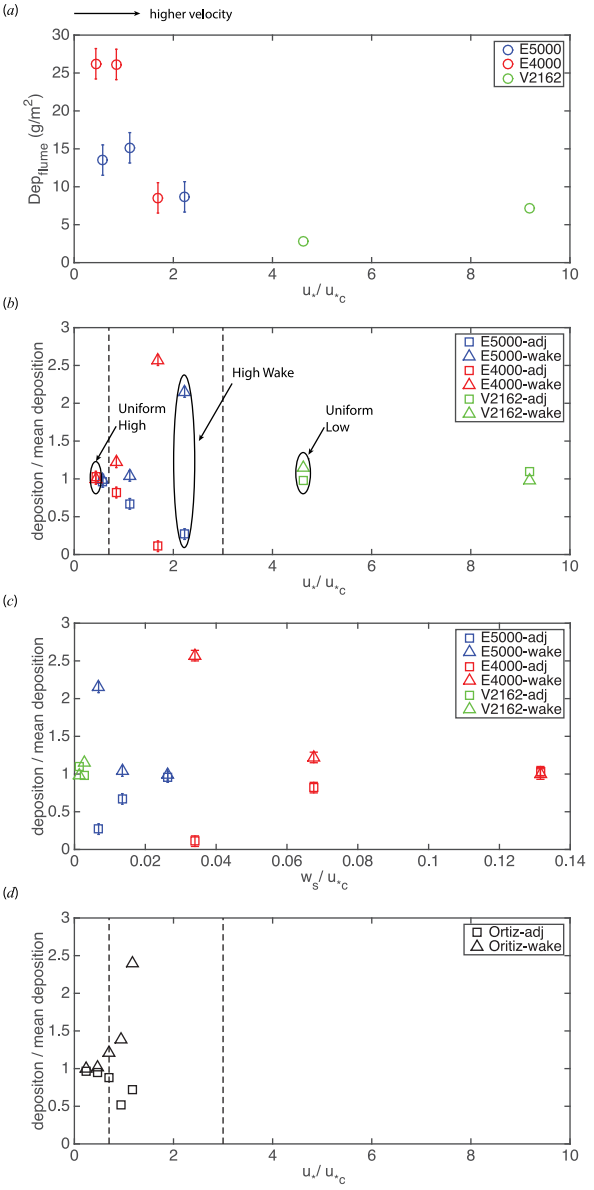

Figure 7. Net deposition versus u_*/u_{*c} and w_s/u_*. (a) Spatially averaged net deposition within the flume (Dep_{flume}) versus u_*/u_{*c}; (b) Deposition in the wake (triangles) and adjacent zones (squares) normalized by the flume spatial average deposition versus u_*/u_{*c}. The labeled ovals identify the deposition patterns discussed in Figure 5 and Figure 6. (c) Nondimensional deposition in the wake and adjacent zones versus w_s/u_*. Uncertainty shown by error bar; (d) Nondimensional deposition in the wake and adjacent zones from *Ortiz et al.* [2013] versus u_*/u_{*c}. Vertical dashed lines in Figures 7b and 7d marked the values $u_*/u_{*c} = 0.7$ and 3, which are the limits for deposition behavior inferred from the available observations.

although just barely so for U_{*wake}. This suggested that resuspension was active throughout the channel, diminishing the net deposition, which was consistent with the low net deposition observed throughout the channel for this case ($Dep_{flume} = 2.8\ gm^{-2}$) and the spatially uniform pattern of deposition (Figure 5b). Finally, for Pattern 3 (high wake deposition for mid weight particle E5000 at 19.6 cm/s), the associated shear velocities are shown in blue in Figure 6. For this case, U_{*wake} (blue triangle) was below u_{*c}, but U_{*adj} (blue square) was above u_{*c}, suggesting that resuspension was active in the adjacent zone but not in the wake zone, which led to elevated net deposition in the wake, relative to the adjacent zone, consistent with the deposition pattern shown in Figure 5c.

Figures 5 and 6 demonstrate that the relative magnitude of local shear velocity and critical shear velocity can delineate whether, or not, a finite patch of vegetation influences the spatial pattern of deposition. This implies that the spatial heterogeneity in net deposition is driven by differences in resuspension (related to u_*/u_{*c}), by inhibiting net deposition in the main channel. Since the distribution of velocity around a patch scales with U_0 (shown in Figures 4b and 4c), the distribution of shear stresses (e.g., U_{*wake} and U_{*adj}) scales with the channel shear velocity u_*, such that u_* can be used as a representative value for the range of shear velocities around the patch. We propose that the ratio u_*/u_{*c} will be a useful metric in predicting the potential influence of a finite patch of vegetation on the distribution of net deposition. To explore this, we plotted all deposition experiments together versus u_*/u_{*c} (Figure 7).

First, the spatial-average net deposition in the flume decreased as u_*/u_{*c} increased (Dep_{flume}, Figure 7a), because as u_*/u_{*c} increased more of the flume bed had a local shear velocity above the threshold for particle resuspension, which diminished net deposition. Second, for $u_*/u_{*c} < 0.7$, there was little difference between the deposition in the wake and in the adjacent zone (Figure 7b), because in both regions the shear velocity was below u_{*c}. In contrast, as u_*/u_{*c} increased, the deposition in the wake and adjacent zones diverged, reaching a maximum difference at $u_*/u_{*c} = 1.6$ (Figure 7b). The range of $u_*/u_{*c} = 0.7$ to 3 corresponded to conditions that produced a divergence between the deposition in the wake and adjacent zones. Over this range $U_{*adj} > u_{*c}$, but $U_{*wake} < u_{*c}$, such that net deposition was higher within the wake and lower within the

adjacent zones. Third, as u_*/u_{*c} increased beyond 3, the deposition in the wake and adjacent zones again converged (Figure 7b), and the mean deposition in the channel reached a minimum (Figure 7a), suggesting that for $u_*/u_{*c} > 3$, deposition was inhibited by high bed shear stress everywhere in the channel, including the wake, leading to a uniform low net deposition. Importantly, it was only within the range $u_*/u_{*c} \approx 0.7$ to 3 that the presence of the vegetation patch significantly influenced the spatial pattern of deposition. Fourth, the maximum deposition in the wake occurred within the range $u_*/u_{*c} \approx 0.7$ to 3, and not at the lowest velocity, as one might expect. Specifically, the maximum Dep_{wake} occurred at $u_*/u_{*c} = 2.38$ for E5000 and at $u_*/u_{*c} = 0.85$ for E4000 (Table 3). Higher deposition in the wake was possible, because resuspension in the adjacent region made more particles available for deposition in the wake, i.e., over the range $u_*/u_{*c} \approx 0.7$ to 3, there was a transfer of particles from the adjacent regions to the wake.

4. Discussion

Ortiz et al. [2013] suggested w_s/u_* as a predictor of spatial heterogeneity in net deposition around a finite patch of vegetation. They showed that as w_s/u_* decreased (or specifically as U_0 increased) the wake and adjacent net deposition diverged [*Ortiz et al*., 2013, Figure 13]. However, their study only considered a single particle size and thus a single value of w_s, and the velocity was not increased enough to reach conditions with resuspension within the wake. We can explore the robustness of w_s/u_*, because both w_s and u_* were varied in our study, and u_* was varied over a wider range. Figure 7c shows that the parameter w_s/u_* did not provide a unique predictor for the divergence between wake and adjacent net deposition. Specifically, the peak divergence between wake and adjacent deposition corresponded to different values of w_s/u_* for different particles. Peak divergence occurred at $w_s/u_* = 0.007$ for E5000 but at $w_s/u_* = 0.04$ for E4000 (Figure 7c). On the other hand, when plotted versus u_*/u_{*c}, the data from *Ortiz et al*. [2013] exhibited a trend consistent with our study (Figure 7d). Specifically, for $u_*/u_{*c} < 0.7$, there was little difference between deposition in the wake and adjacent zones; but for $u_*/u_{*c} > 0.7$, the wake and adjacent zone deposition diverged, with divergence reaching a peak when u_*/u_{*c} approached the value of 1.3, which was consistent with the ratio at which our data exhibited a peak divergence (Figure 7b). The similarity between Figures 7b and 7d reinforces the point that the spatial variation in net deposition was driven by the inhibition of deposition by resuspension in the open channel (associated with $u_*/u_{*c} > \approx 1$).

Previous studies have suggested that the wakes behind vegetation and woody debris are regions of fine-particle deposition that promote additional growth and elongation of the vegetated region [e.g., *Tsijimoto*, 1999; *Gurnell et al*., 2001, 2008]. This study has provided additional insight into this process by demonstrating that the vegetation-deposition feedback depends on channel velocity, and specifically that a positive feedback with enhanced net deposition in the wake only occurs over a limited range of channel velocity that is dependent upon the particle density and size, as reflected in u_{*c}. Specifically, the wake region will preferentially collect fine material, relative to the adjacent open channel, only when the adjacent shear velocity is above the critical shear velocity and the wake shear velocity is below this threshold. This points to a necessary modification in the landscape evolution model presented by *Kondziolka and Nepf* [2014], which assumed that particle deposition promoting new growth was possible for all velocity conditions, i.e., particle supply to the wake was unlimited. Our study demonstrates that an additional control is needed in the Kondziolka model, so that enhanced deposition in the wake would only occur when resuspension was present in the adjacent open channel. Our study suggests that these conditions occur when u_*/u_{*c} is of the order of 1, or, specifically between 0.7 and 3. Importantly, we observed that this range of flow conditions produced the highest net deposition in the wake, exceeding net deposition at lower velocities (lower u_*/u_{*c}, Table 3), because the resuspension (or inhibition of deposition) in the adjacent regions of the open channel provided additional material to the wake. For higher velocity (specifically $u_*/u_{*c} > 3$), deposition was inhibited in the wake as well as the channel, so that no spatial pattern in deposition occurred. Finally, if the velocity is too low, such that resuspension is eliminated in the channel as well as the wake, there is no difference in deposition between the adjacent zone and the wake, and the wake does not benefit from an additional supply of resuspended sediment from the adjacent open channel.

Each experiment in the present study considered a single particle size. However, field sites typically have a range of particle sizes. If there is a mixture of particle sizes, our study suggests that some particle sizes will preferentially deposit in the wake, i.e., those for which u_{*c} falls between 0.3 u_* and 1.4 u_* (corresponding to $u_*/u_{*c} \approx 0.7$ to 3). That is, for a particular channel velocity, a particular range of particles should segregate into the wake. This conclusion is supported by a recent study of sediment transport around a patch of

Table 4. Shear Velocity Ratio u_*/u_{*c} Calculated for Sediment and Flow Conditions Used in *Waters* [2014][a]

	Grain Size (mm)		
u_*/u_{*c}	0.063	$d_{50} = 0.55$	6.3
High flow [$u_* = 0.022$ m/s]	2.0	1.3	0.4
Low flow [$u_* = 0.016$ m/s]	1.4	1.0	0.6

[a]The following data were reported in figures and Tables included in *Waters* [2014]: flow rate (Figure 3.5.2); flow depth (Table 8.3.1); grain sizes (Figure 3.6.1); and channel width was 0.6m (p. 95).

model vegetation with solid volume fraction, $\phi = 0.10$, similar to our study, $\phi = 0.13$ [*Waters*, 2014]. At the start of the experiment, the bed consisted of a uniform mixture of sand and gravel, with particle sizes between 0.063 and 6.3 mm, and $d_{50} = 0.55$mm. After running several flood hydrographs, the grain size within the wake behind the patch decreased by 20%, because finer particles had preferentially accumulated in the wake [*Waters*, 2014, Figure 7.3.2]. The sorting of finer material into the wake is consistent with the range of u_*/u_{*c} estimated for the channel. Using the same method discussed in section 2.3, u_{*c} was calculated for the maximum, minimum, and d_{50} of the original channel mixture (Table 4). The peak channel velocity was estimated for the high and low flow rate conditions reported in Figure 3.5.2 of *Waters* [2014], using the corresponding flow depth [*Waters*, 2014, Table 8.3.2]. The shear velocity u_* was then estimated from equation (6.14) and Table 6.1 in *Julien* [1995], using $d_{50} = 0.55$mm. This analysis revealed that the finer grain sizes ($d \leq d_{50}$) fell in the range $u_*/u_{*c} = 0.7$ to 3, but for the largest grain size $u_*/u_{*c} < 0.7$ (Table 4), so that our parameterization predicts that only the smaller grain sizes would partition into the wake, which would lead to a decrease in d_{50} within the wake, consistent with Waters' observations. Similarly, *Tanaka and Yagisawa* [2010] noted that the material deposited in the wake behind a natural patch of vegetation consisted of finer grains than were observed upstream of the patch, suggesting that finer particles were preferentially resuspended and relocated into the wake, which is also consistent with our model. Unfortunately, velocity was not reported by *Tanaka and Yagisawa* [2010], so we cannot calculate the ratio of u_*/u_{*c} for a more quantitative comparison.

The particular threshold values for u_*/u_{*c} will depend on patch flow blockage (aD), which determines the velocity in the wake, U_1 [*Chen et al*. 2012]. In this study, $aD = 5.1$, which is in the high flow blockage regime ($aD > 4$), for which the velocity in the wake is less than 10% of the upstream velocity. Because U_1/U_0 has little variation for high flow blockage [see *Chen et al*., 2012], the thresholds found in this study would likely apply for any high flow blockage patch. However, in the low flow blockage regime ($aD < 4$), the velocity in the wake may not be significantly diminished, e.g., for $aD = 2$, $U_1/U_0 = 0.6$ [Figure 8 in *Chen et al*., [2012], and therefore these wakes will be less effective at capturing fine particles. Specifically, a smaller value of u_*/u_{*c} will likely be needed to drive the wake shear velocity low enough to enhance deposition in the wake (Pattern 3), such that enhanced deposition in the wake will occur over a narrower range of u_*/u_{*c}. If the vegetation is flexible, but effectively emergent, the flow adjustment and limits of depositional behavior should be the same as reported here. However, if the vegetation is flexible and submerged, the wake behind the patch could be quite different and the threshold for the different deposition patterns would likely shift. In particular, submerged vegetation generates a vertical shear layer in the patch wake with associated vertical recirculation that may inhibit deposition in the wake (e.g., as shown in *Ortiz et al*. [2013]).

5. Conclusions

Because of the additional flow resistance provided by vegetation, flow is diverted laterally around an emergent patch, so that the velocity is enhanced in the region adjacent to the patch and diminished directly downstream from the patch. Previous studies have suggested that this spatial pattern of velocity influences the spatial pattern of net deposition [e.g., *Bouma et al*., 2007; *Chen et al*., 2012; *Ortiz et al*., 2013]. Our study has shown that this feedback between vegetation and deposition only occurs over a limited range of flow and particle conditions, defined by the ratio of channel shear velocity to critical shear velocity, u_*/u_{*c}, which is a metric similar to the ratio of shear stress to critical shear stress. When $u_*/u_{*c} < 0.7$ (low velocity or large, heavy particles), the shear velocity everywhere in the channel is below the critical shear velocity, and resuspension is shut off everywhere in the channel, resulting in uniform high net deposition. Similarly, for $u_*/u_{*c} > 3$ (high velocity or small, light particles), resuspension is active everywhere in the channel, producing uniform low net deposition. It is only within the range $u_*/u_{*c} \approx 0.7$ to 3 that the presence of the vegetation patch creates a significant spatial pattern of net deposition different from the control with no patch. Specifically, higher net deposition occurs in the wake than in the adjacent regions. Importantly, the maximum net deposition in the wake occurs within this range of

conditions, because resuspension in the adjacent regions makes more particles available for deposition in the wake. Comparison to mixed bed studies [*Tanaka and Yagisawa*, 2010; *Waters*, 2014] suggests that the ratio u_*/u_{*c} can be used to predict the preferential accumulation of fine particles in the wake behind a finite patch of vegetation.

Acknowledgments
The velocity data are available in excel format upon request from the authors. Data supporting Figure 6 and 7 are available in Table 3. Data for Figure 7d were provided by Alejandra C. Ortiz and Heidi M. Nepf. Y. Shi and B. Jiang were supported by funds from the China Scholarship Council. Funding for the experiments was provided by NSF EAR-1414499.

References

Bos, A. R., T. J. Bouma, G. L. J. de Kort, and M. M. van Katwijk (2007), Ecosystem engineering by annual intertidal seagrass beds: Sediment accretion and modification, *Estuarine Coast. Shelf Sci.*, *74*(1–2), 344–348, doi:10.1016/j.ecss.2007.04.006.

Bouma, T. J., L. A. van Duren, S. Temmerman, T. Claverie, A. Blanco-Garcia, T. Ysebaert, and P. M. J. Herman (2007), Spatial flow and sedimentation patterns within patches of epibenthic structures: Combining field, flume and modelling experiments, *Cont. Shelf Res.*, *27*, 1020–1045, doi:10.1016/j.csr.2005.12.019.

Chen, Z., A. C. Ortiz, L. Zong, and H. M. Nepf (2012), The wake structure behind a porous obstruction and its implications for deposition near a finite patch of emergent vegetation, *Water Resour. Res.*, *48*, W09517, doi:10.1029/2012WR012224.

Cotton, J. A., G. Wharton, J. A. B. Bass, C. M. Heppell, and R. S. Wotton (2006), The effects of seasonal changes to in-stream vegetation cover on patterns of flow and accumulation of sediment, *Geomorphology*, *77*, 320–334, doi:10.1016/j.geomorph.2006.01.010.

Crowder, D. W., and P. Diplas (2000), Using two-dimensional hydrodynamic models at scales of ecological importance, *J. Hydrol.*, *230*, 172–191, doi:10.1016/S0022-1694(00)00177-3.

de Lima, P. H. S., J. G. Janzen, and H. M. Nepf (2015), Flow patterns around two neighboring patches of emergent vegetation and possible implications for deposition and vegetation growth, *Environ. Fluid Mech.*, *15*(1), 1–18, doi:10.1007/s10652-015-9395-2.

Follett, E. M., and H. M. Nepf (2012), Sediment patterns near a model patch of reedy emergent vegetation, *Geomorphology*, *179*, 141–151, doi:10.1016/j.geomorph.2012.08.006.

Gurnell, A. M. (2014), Plants as river system engineers, *Earth Surf. Processes Landforms*, *39*, 4–25, doi:10.1002/esp.3397.

Gurnell, A. M., G. E. Petts, D. M. Hannah, B. P. G. Smith, P. J. Edwards, J. Kollmann, J. V. Ward, and K. Tockner (2001), Riparian vegetation and island formation along the greavel-bed Fiume Tagliamento, Italy, *Earth Surf. Processes Landforms*, *26*, 31–62.

Gurnell, A. M., K. Thompson, J. Goodson, and H. Moggridge (2008), Propagule deposition along river margins: Liking hydrology and ecology, *J. Ecol.*, *96*, 553–565, doi: 10.1111/j.1365-2745.2008.01358.x.

Gurnell, A. M., W. Bertoldi, and D. Corenblit (2012), Changing river channels: The roles of hydrological processes, plants and pioneer fluvial landforms in humid temperate, mixed load, gravel bed rivers, *Earth Sci. Rev.*, *111*(1–2), 129–141, doi:10.1016/j.earscirev.2011.11.005.

Hafs, A. W., L. R. Harrison, R. M. Utz, and T. Dunne (2014), Quantifying the role of woody debris in providing bioenergetically favorable habitat for juvenile salmon, *Ecol. Modell.*, *285*, 30–38, doi:10.1016/j.ecolmodel.2014.04.015.

Jones, J. I., A. L. Collins, P. S. Naden, and D. A. Sear (2012), The relationship between fine sediment and macrophytes in rivers, *River Res. Appl.*, *28*(7), 1006–1018, doi:10.1002/rra.1486.

Julien, P. Y. (1995), *Erosion and Sedimentation*, Cambridge Univ. Press, N. Y.

Kondziolka, J. M., and H. M. Nepf (2014), Vegetation wakes and wake interaction shaping aquatic landscape evolution, *Limnol. Oceanogr. Fluids Environ.*, *4*, 106–119, doi:10.1215/21573689-2846314.

Kouwen, N., and T. E. Unny (1975), Flexible roughness in open channels, *J. Hydraul. Div. Am. Soc. Civ. Eng.*, *101*(NHY1), 194–196.

Lamb, H. (1993), *Hydrodynamics*, Cambridge Univ. Press, N. Y.

Leonard, L. A., and M. E. Luther (1995), Flow hydrodynamics in tidal marsh canopies, *Limnol. Oceanogr.*, *40*(8), 1474–1484, doi:10.4319/lo.1995.40.8.1474.

Lightbody, A. F., and H. M. Nepf (2006), Prediction of velocity profiles and longitudinal dispersion in salt marsh vegetation, *Limnol. Oceanogr.*, *51*(1), 218–228, doi:10.4319/lo.2006.51.1.0218.

Marion, A., et al. (2014), Aquatic interfaces: A hydrodynamic and ecological perspective, *J. Hydraul. Res.*, *52*, 744–758, doi:10.1080/00221686.2014.968887.

Meire, D. W. S. A., J. M. Kondziolka, and H. M. Nepf (2014), Interaction between neighboring vegetation patches: Impact on flow and deposition, *Water Resour. Res.*, *50*, 2108–2123, doi:10.1002/2012WR013085.

Nepf, H. M. (2012), Flow and transport in regions with aquatic vegetation, *Annu. Rev. Fluid Mech.*, *44*, 123–142, doi:10.1146/annurev-fluid-120710-101048.

Ortiz, A. C., A. Ashton, and H. M. Nepf (2013), Mean and turbulent velocity fields near rigid and flexible plants and the implications for deposition, *J. Geophys. Res. Earth Surf.*, *118*, 2585–2599, doi:10.1002/2013JF002858.

Rominger, J. T., and H. M. Nepf (2011), Flow adjustment and interior flow associated with a rectangular porous obstruction, *J. Fluid Mech.*, *680*, 636–659, doi:10.1017/jfm.2011.199.

Rominger, J. T., A. F. Lightbody, and H. M. Nepf (2010), Effects of added vegetation on sand bar stability and stream hydrodynamics, *J. Hydraul. Eng.*, *136*(12), 994–1002, doi:10.1061/(asce)hy.1943-7900.0000215.

Schulz, M., H. P. Kozerski, T. Pluntke, and K. Rinke (2003), The influence of macrophytes on sedimentation and nutrient retention in the lower River Spree (Germany), *Water Res.*, *37*, 569–578, doi:10.1016/S0043-1354(02)00276-2.

Stephan, U., and D. Gutknecht (2002), Hydraulic resistance of submerged flexible vegetation, *J. Hydrol.*, *269*(1–2), 27–43, doi:10.1016/S0022-1694(02)00192-0.

Tanaka, N., and J. Yagisawa (2010), Flow structures and sedimentation characteristics around clump-type vegetation, *J. Hydro-environ. Res.*, *4*(1), 15–25, doi:10.1016/j.jher.2009.11.002.

Tsujimoto, T. (1999), Fluvial processes in streams with vegetation, *J. Hydraul. Res.*, *37*(6), 789–803, doi:10.1080/00221689909498512.

Valiela, I., J. Teal, and W. Deuser (1978), The nature of growth forms in the salt marsh grass Spartina alterniflora, *Am. Nat.*, *112*(985), 467–470.

Waters, K. A. (2014), Sediment transport dynamics around an emergent vegetation patch in unsteady flows, PhD dissertation, Sch. of Eng. and Appl. Sci., Univ. of Va., Charlottesville.

White, B. L., and H. M. Nepf (2007), Shear instability and coherent structures in shallow flow adjacent to a porous layer, *J. Fluid Mech.*, *593*, 1–32, doi:10.1017/S0022112007008415.

Zong, L., and H. M. Nepf (2010), Flow and deposition in and around a finite patch of vegetation, *Geomorphology*, *116*, 363–372, doi:10.1016/j.geomorph.2009.11.020.

Zong, L., and H. M. Nepf (2011), Spatial distribution of deposition within a patch of vegetation, *Water Resour. Res.*, *47*, W03516, doi:10.1029/2010WR009516.